

# RSC Advances



This is an *Accepted Manuscript*, which has been through the Royal Society of Chemistry peer review process and has been accepted for publication.

*Accepted Manuscripts* are published online shortly after acceptance, before technical editing, formatting and proof reading. Using this free service, authors can make their results available to the community, in citable form, before we publish the edited article. This *Accepted Manuscript* will be replaced by the edited, formatted and paginated article as soon as this is available.

You can find more information about *Accepted Manuscripts* in the [Information for Authors](#).

Please note that technical editing may introduce minor changes to the text and/or graphics, which may alter content. The journal's standard [Terms & Conditions](#) and the [Ethical guidelines](#) still apply. In no event shall the Royal Society of Chemistry be held responsible for any errors or omissions in this *Accepted Manuscript* or any consequences arising from the use of any information it contains.

Cite this: DOI: 10.1039/c0xx00000x

www.rsc.org/xxxxxx

Paper

# From 1D to 3D: A New Route to Fabricate Tridimensional Structure via Photo Generation of Silver Networks

Huaizhong Shen,<sup>a</sup> Yuxin Wu,<sup>a</sup> Liping Fang,<sup>a</sup> Shunsheng Ye,<sup>a</sup> Zhaoyi Wang,<sup>a</sup> Wendong Liu,<sup>a</sup> Zhongkai Cheng,<sup>a</sup> Junhu Zhang,<sup>a</sup> Zhanhua Wang\*<sup>b</sup> and Bai Yang\*<sup>a</sup>

Received (in XXX, XXX) Xth XXXXXXXXXX 20XX, Accepted Xth XXXXXXXXXX 20XX

DOI: 10.1039/b000000x

A rapid and cost effective method has been developed to fabricate 3 dimensional (3D) ordered structure by photo generating silver networks inside a 1D layered heterogeneous lamination composing of poly(vinyl alcohol) (PVA) and poly(methyl methacrylate) (PMMA). By designing the photo mask meticulously, the silver nanoparticles (NPs) produced by UV light aggregate to form frameworks in different ways which perform as the anisotropic component, i.e. the building blocks thus convert the 1D structure into 3D. Formation of silver NPs increases the refractive index (RI) of PVA layers, thus brings optical change to the 1D laminar structure which allows us to trace the silver formation process by measuring the change of RI value and reflectance spectra. The 1D layered structure acts as a good building matrix for 3D construction for that the total number of layers and the layer thickness can be finely tuned flexibly which allow us further study the various properties brought by the structural modulation. By utilizing the photo-reactive silver ions, an innovative strategy of fabricating 3D structure through *in-situ* photo-generating silver building blocks inside the laminar matrix is settled, which make it possible for fabricating 3D micro/nano composite materials with potential applications in the fields such as sensor and photonic *meta*-materials.

## Introduction

Inspired by the typical structures existing in nature creatures,<sup>1-5</sup> three dimensional ordered structure, of which the constituent component is orderly distributed in three dimension, has drawn much attention from researchers due to its special applications in manipulating the light propagation,<sup>6</sup> cell differentiation<sup>7</sup> and potential use in *meta*-materials.<sup>8, 9</sup> 3D structures consisting of self-assembly colloidal spheres will exhibit vivid and bright structural color<sup>10</sup> which derived from the interference effects within their periodic distribution of the building blocks, while the 3D structure containing unit cells which are much smaller than the wavelength of light will present many new and unusual optical properties.<sup>8</sup> As the structure evolves, many new properties and applications are discovered and studied. Thus, constructing 3D structures with different forms is highly required.

High resolution top-down approaches as well as bottom-up technologies have been developed including electron-beam lithography,<sup>11</sup> ion beam lithography,<sup>12</sup> direct laser writing,<sup>13</sup> and self-assembly<sup>14-18</sup> to construct 3D structures in multiple scales. For instance, researchers have successfully fabricated various 3D patterns and networks to be used as cell guidance scaffolds,<sup>19</sup> tissue engineering matrix<sup>20</sup> and biomimetic manufacturing.<sup>21</sup> Another category of 3D structures of great importance is the

photonic *meta*-materials, which are man-made structures consisting of repeating periodic micro- or nanostructured metalodielectric building blocks. Since the first introduction around one decade ago,<sup>22</sup> photonic *meta*-material have been on its fast evolution to smaller and more delicate.<sup>23, 24</sup> By precisely designing the patterns' shape, geometry, size, orientation and arrangement ahead of fabrication and combining the sophisticated top-down manufacture process, the photonic *meta*-materials possess novel electromagnetic properties such as negative refractive index, perfect absorption and negative magnetic permeability, which are not exist in nature.<sup>25</sup> There are also previous reviews summarizing the fabrication methods of *meta*-material.<sup>26-30</sup> Among them, layer deposition technique which involves pattern making in single layer and subsequently stacking process is widely used to fabricate stacked 3D *meta*-material. However, there remain challenges in the construction of such 3D structure.<sup>31</sup> One is the repeated stacking of unit cells to qualify the structure as a real material, the other is to realize various styles of the building blocks which has an obvious influence on the structure's magnetic resonance frequency. Besides, the sophisticated technology and equipments involved in the fabrication process also increase the complexity and the cost. Hence, to exploit an easy and economical way to fabricate 3D ordered structure is of great importance.

From the above-mentioned applications we noticed one thing that

in the cases both biology and photonic regulation, the 3D structures involve repeating patterned layer stacks, which are most likely a post-processed 1D layered structure. This enlightens us that whether we can fabricate a 1D heterogeneous layered structure at the first step, then convert it into 3D through post-processing such as chemical reaction inside the layer stacks. Based on the analysis above, polymeric 1D layers and metal ions-contained polymer films enter our field of vision. Previous studies prove that light-induced reduction of metal ions embedded in polymer films is effective and well-conducted.<sup>32-34</sup> Among them, *in-situ* reduction of silver ions is studied extensively by scientists for its mild reactive chemistry in solid phase.<sup>35, 36</sup> Mills and coworkers develop a method to produce silver nanoparticles (NPs) and clusters in crosslinked PVA/PAA films.<sup>37</sup> Ozin group incorporate silver NPs into the TiO<sub>2</sub>/clay layers to modify the photonic properties.<sup>38</sup> Nesbitt et al. further study the experimental protocols, reaction process and morphology of photo-generated Ag NPs.<sup>39</sup> Besides, silver ions embedded in polymer films can be selectively reduced to aggregate into different 2D and 3D structure possibly through combining with photomasks or direct laser writing technology which provides a route for photo-patterning.<sup>40, 41</sup> Furthermore, Ag NPs presents high catalytic activity,<sup>42</sup> anti-bacteria ability<sup>43</sup> and other potential use such as in SERS for its characteristic of surface plasmon resonance,<sup>44, 45</sup> which may bring new functions to the ordered structure. For the reasons we mentioned above, silver NPs can be utilized to form building blocks for 3D construction beginning with 1D layer structure as building matrix. In this paper, we first fabricated a polymer heterogeneous 1D layered structure doped with silver ions. By selectively reducing Ag<sup>+</sup> in specific part of the 1D layered stacks, 3D networks of Ag were formed inside the structure making it turned out to be a 3D construction based on the heterogeneous polymer lamination, which is an exemplified combination of top-down and bottom-up fabrication. By increasing the refractive index (RI) of PVA layer, silver NPs strongly modified the optical properties of the 1D stack with an obvious photonic band gap (PBG) within 3 bilayers which provides us a chance to trace the silver reduction process by measuring reflectance and RI value of the composite film. Modulation of the structural parameters of the 1D matrix such as period and number of layers can be achieved, this further enables us the fine adjustment of the 3D structure. Finite-Difference Time-Domain (FDTD) simulation was also conducted to confirm our results. Our method realizes the successful combinatorial construction of 1D layers matrix and photo-generation silver building blocks to form 3D ordered structure which give possibilities to the potential applications in bioassays, SERS matrix and photonic *meta*-materials.<sup>6-9</sup>

## Results and discussion

### Building of 3D structure

The process of constructing the 3D ordered structure is illustrated in Figure 1. Briefly, the 3D structure is fabricated by exposing the as prepared Ag<sup>+</sup> doped 1D heterogeneous layer stacks to UV irradiation with pre-designed mask in which process that the *in-situ* photo reduction of silver ions happen in specific area inside the laminar structure, leading to the formation of composite 3D

polymer-silver NPs hybrid materials. Compared to traditional fabrication methods of building stacked 3D material which may involve sophisticated instruments or complicated process, our approach is to generate building blocks after the acquirement of a layered structure. The alignment of the building blocks belonging to different layers is achieved by the rectilinear propagation of UV light which is guaranteed by carefully selecting the irradiation source matching the scale of patterns to avoid the diffraction. Unlike the layer deposition technique we mentioned above, this method omits the time-consuming process such as aligning marker making, lateral aligning and planarization<sup>46</sup>.

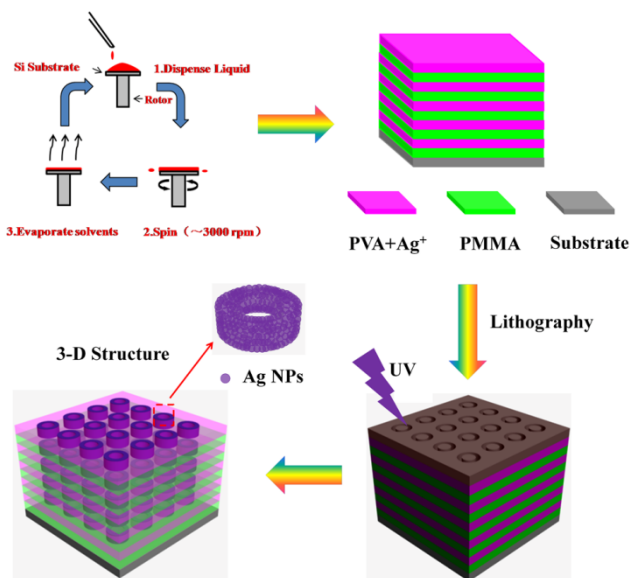


**Fig. 1** Schematic representation of the construction of 3D structure derived from Ag ions doped 1D heterogeneous laminar stacks.

Various building blocks can be produced by utilizing different photo masks. Layered stacks may support smaller periods and the distance between building blocks can be adjusted by changing the internal film thickness which we will discuss in detail in the following parts. Besides, we make the silver-contained sol ahead of film fabrication which affords an accurate control of the amount of metal ions in the film over large area. However, there are also limits in the utilization of such method. One is that because of the laminar character and unlike the direct laser writing producing 3D building blocks directly, this method is suitable to fabricate stacked 3D structure. The other is that the size of building blocks is limited by the mask and irradiation source. Apart from the disadvantages above, fabricating 1D layers ahead of producing building blocks still provide us an alternative way to construct stacked 3D structure.

### Zero-Valent silver NPs are formed during UV exposure

To verify the formation of silver NPs during the UV exposure, samples exposed to UV light directly without masks are taken into tests. The reflectance spectrum of a 3-bilayer sample in initial state is shown in Figure 2a (black line). While after 30 min UV irradiation, an intense peak (around 76% reflectance for 1D layered stacks consist of 3 bilayers) is observed at 630 nm (Figure 2b, black line), the reflectance ranging from 400 to 500 nm decrease dramatically compared to initial state. We suspect that as a high-refractive index value component, silver NPs

embedded in the PVA film bring optical change to the 1D layer system. The refractive index for PMMA and Ag<sup>+</sup> contained PVA polymer layer is 1.474 and 1.481 respectively. The small difference between these two layers makes it difficult to achieve a photonic band within 3 bilayers.<sup>47, 48</sup> However, the silver NPs increased the refractive index of PVA polymer films and the contrast between these two polymer films dramatically, thus satisfied all the conditions for being a typical one dimensional photonic crystal (1DPC) with an obvious photonic band. Strong absorption centered at 430-450 nm have been reported for silver contained PVA films,<sup>37</sup> which may result in the reflection intensity decrease in the wavelength range of 400 to 500 nm. FDTD simulation was conducted here to confirm the experimental reflectance spectra (Figure 2a, 2b, red lines). The parameters (refractive index, film thickness, number of layers, component material, incident angle) we used are based on our test

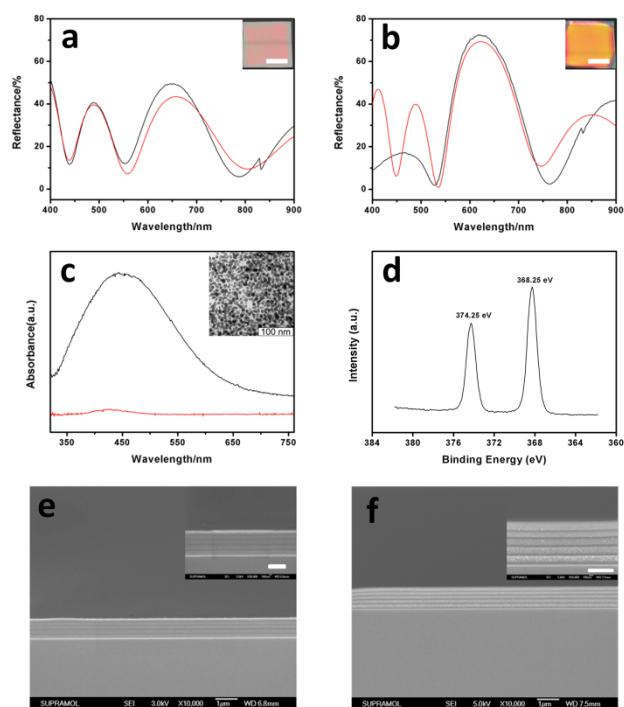


**Fig. 2** Reflectance spectra of a 3-bilayer sample before (a) and after (b) UV irradiation (black lines). Red lines are corresponding calculated results by FDTD simulation. Insets are the photographs of the samples in corresponding state, the scale bar is 1 cm. (c) *ex-situ* absorbance spectrum of Ag NPs composite films, red line represents the sample before UV exposure while black line is the same sample after UV exposure, inset is the TEM image of the silver NPs formed inside the films. (d) Ag 3d XPS spectrum of the silver NPs embedded PVA films. Cross sectional SEM images of the 1D layer stacks before (e) and after (f) UV curing, insets are corresponding magnified images, the scale bar for inset images is 500 nm.

results. Our experimental spectra (peak position and intensity) matched the simulation results very well except for the wavelength range of 400 to 540 nm in figure 2b which should be attributed to the difference between the simulation model and practical situation. In practice, the increase of RI value of PVA film is induced by the embedded silver NPs. However, in the FDTD simulation, we establish a model of high and low RI value distribution instead of a metal-polymer composite film, thus surface plasmon resonance (SPR) absorption is not taken into

consideration. That is the reason why the reflectance intensity is stronger in the simulated spectrum (figure 2b, red line). The sample after UV exposure exhibits uniform and bright color (Figure 2b) compared to that without UV curing (Figure 2a) which should be ascribed to the strong reflectance around 630 nm. The polymer-silver NPs composite film was studied by an *ex-situ* measurement of absorption spectrum. The single film exhibits an intense absorption centered at 450 nm (Figure 2c) after UV exposure for 10 min under a mercury lamp (500 W,  $\lambda=365$  nm), which resulted from the Ag<sup>0</sup> particles SPR absorbance.<sup>37</sup> The morphology of Ag NPs was characterized by TEM images. TEM samples were acquired from the same single film by immersing the quartz based PVA film into HF/H<sub>2</sub>O (volumetric ratio =1:9, caution: highly corrosive!) mixture for 10 s, and then lift up a small piece of the single film with a carbon support film. Monodisperse silver NPs with an average diameter of 10 nm were observed (original TEM image is shown in figure S2). In comparison to the particles in aqueous solution, the movements and aggregation of NPs were confined in the solid film. This contributes to the monodispersity of the silver NPs. The X-ray photoelectron spectroscopy (XPS) Ag 3d spectrum of the Ag-contained PVA composite films were analyzed which further confirmed the reduction to form Ag<sup>0</sup>. As shown in Figure 2d, the binding energy of the Ag 3d was observed at 368.25 eV and 374.25 eV with a spin energy separation of 6.0 eV which would correspond to Ag (0), indicating that the silver ions are mostly reduced to metallic silver nanoparticles during the UV exposure.<sup>49</sup> The cross sectional structure of the 1D laminar stacks before and after UV curing was shown in Figure 2e and Figure 2f. There were sharp interfaces between the layers representing a typical morphology of a 5 double-layer stacks. Film thickness of PVA and PMMA layer was 142 nm and 53 nm respectively, which are in accordance with the results measured by surface profiler and auto-laser ellipsometer. The choice for solvents is crucial for the successful building of the 1D multilayer structure, as we mentioned in the experimental part, we should always avoid the mutual dissolution and penetration between different layers. Ag NPs embedded in PVA films were clearly shown in Figure 2f. The size of the particles embedded in bottom layers is relatively larger than those in the upper layers, this can be explained by the nucleation and crystal growth theory.<sup>50, 51</sup> The growth typically follows an initial stage of nucleation, the amount of the nucleus formed in the upper layers is larger than that in the bottom layers for the UV light need to penetrate the upper stacks to reach the bottom ones which resulted in the size increase from the surface to the inner layers.

### Silver networks are obtained after UV curing under photomask

The photo reactive silver ions inside 1D layered heterogeneous structure open a new way to build 3D network structure. Making use of the chemical reaction of Ag<sup>+</sup> under the external UV light,<sup>52</sup> 3D structure was obtained instead of sophisticated physical management. By selectively reducing the Ag<sup>+</sup> in specific part, different frameworks were formed according to the pre-designed photo mask. As can be seen from Figure 3a, stripped pattern with the size of 10 micrometer ( $\mu$ m) was observed under microscope. During the exposure, the sample protected by the mask remained the initial state, while the part without protection converted to

zero valence Ag which changed the optical properties thus made the color contrast. With the same method, we also produced dots, concentric annulus, triangles and English letters on our samples. The size, shape and interval distance all can be modulated by previous designing of the photo masks. The smallest part of the letter K in the word key (Figure 3e) is 8  $\mu\text{m}$  while the thinnest part in letter D in DNA (Figure 3f) is 2  $\mu\text{m}$  which indicates that we can precisely modulate the pattern size in minimum scale around 5 micrometer. Besides micro pattern fabrication, we also write macro letters by UV light in this multilayer matrix (Figure S1). JLU was written in a 2 $\times$ 2 cm silicon substrate and the reflectance spectra of the letter and blank space was measured respectively. The part exposed to UV light formed the JLU pattern through Ag<sup>0</sup> generation which produce photonic stop band centered at 600 nm. The cross sectional SEM measurement was conducted along the border of the adjacent letter and blank space. As can be seen in Figure S3, there is obvious difference in the amount of silver NPs along the

reduced in NPs barren region. However, the UV light accelerate the reduction process thus forming the NPs rich part. The difference in reaction rates also clearly verified the effectivity of modulating UV light to produce silver networks in selective part

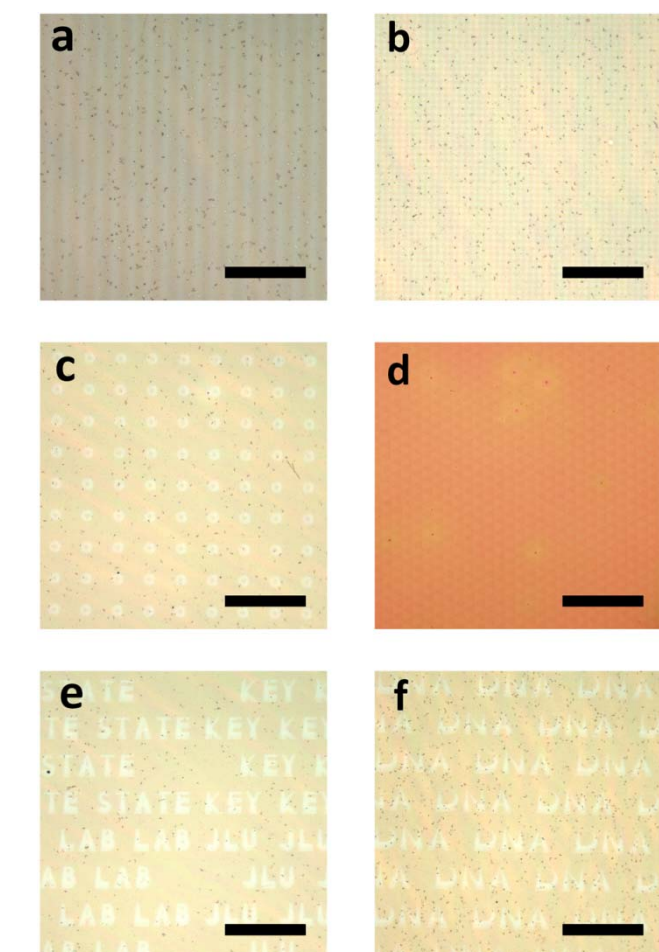


**Fig. 3** a) Micrographs of the sample with a) stripe, b) dot, c) concentric annulus, d) triangle and e-f) English letters from top view, scale bar are all 200  $\mu\text{m}$  except for Figure 3a is 100  $\mu\text{m}$ .

fracture surface, which we defined as NPs barren and NPs rich part. The NPs rich part belong to letter J while the NPs barren part belong to the neighbouring space which protected by the photomask. Previous study by Mills and co-workers reported that silver ions can be reduced by PVA in dark,<sup>37</sup> which explains why even with the shield of photomask, the silver ions are partly

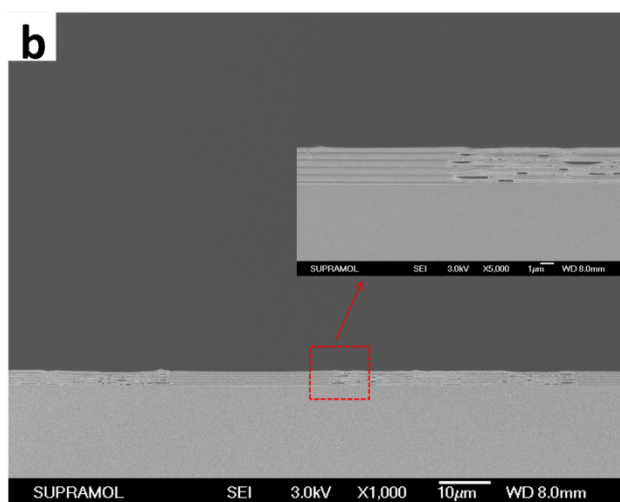
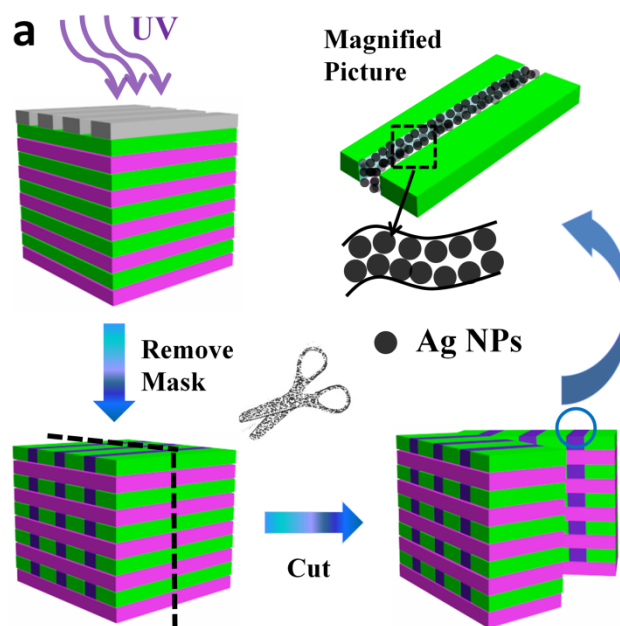


**Fig. 4** a) Schematic illustration of the inner structure derived from a sample exposed to UV light with a stripe mask, b) Cross sectional SEM image of a illustrational sample with stripes pattern. It appears periodical smooth and wrinkle morphology which corresponds to the photo mask we used.

of the 1D matrix. However, the silver ions remaining in the part with protection of photomasks may be reduced slowly when exposed to daily light. Even though this is a slow process when compared to the reduction under UV exposure, it may lead to the degradation of the as-prepared silver networks which is a problem remained to be solved. A possible solution is adding a rinsing step after UV exposure to release the silver ions embedded in the polymer films. Considering that PVA film is hydrophilic, water may infiltrate and then dissolve the ions which is similar to a process described in a previous study.<sup>53</sup> However, this needs more experiments to further verify and avoiding

further damage to the PVA films. The distance of zero-valence Ag belonging to different PVA layers also can be modulated by changing the thickness of PMMA layers, which we will discuss in the following parts.

Figure 2f verifies that the UV light can penetrate the whole stacks and reach the bottom layer to conduct silver ions reduction which indicates that the patterns we get above are not confined to the surface. Here, we take the sample with stripe pattern for example to study the morphology inside the structure. For preparing the SEM sample, a photo mask with 30  $\mu\text{m}$  transparent and 50  $\mu\text{m}$  opaque region was utilized, and to match the scale of the mask, we specially fabricated a 1D structure with thicker layers (PVA 415 nm, PMMA 125 nm). Figure 4a shows the illustrational

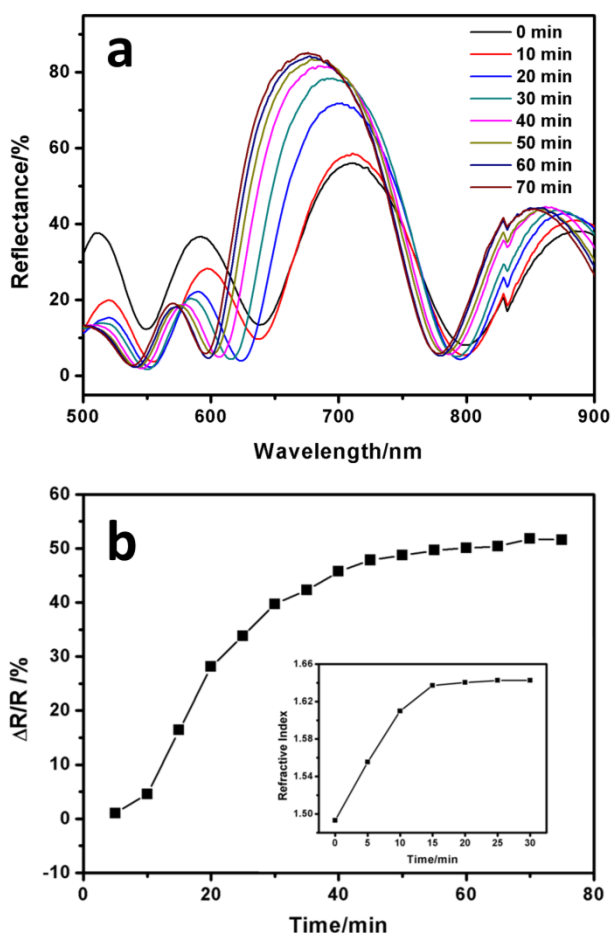


**Fig. 5** a) Time-dependent reflectance spectra of the silver doped laminar stacks. b) Time-dependent change of reflectance intensity, inset is the increase of refractive index of a single composite film during UV curing.

process of the formation of silver building blocks. Zero valent silver NPs formed after exposed to UV light and then aggregate according to the mask's shape. Corresponding cross sectional SEM image of the as prepared sample is shown in Figure 4b. It appears periodical smooth and wrinkle morphology along the fracture surface and the difference between these two parts is so obvious that it could be easily identified. This should be ascribed to the mechanical property change brought by the Ag NPs. Because of the ductility of the polymer, the edges of the polymer tended to stretch after fracture, while for the body containing

silver NPs, the rigidity increased which contributed to the sharp interfaces. The length of smooth and wrinkle part is 30  $\mu\text{m}$  and 50  $\mu\text{m}$  respectively which correspond to the photo mask. For smaller stripes with 10  $\mu\text{m}$  alternatively distribution, the cross sectional SEM images was shown in Figure S4. The same morphology of periodical wrinkle and smooth distribution was also found which correspond to the size scale of the mask. The part without protection of photomask exhibited smooth morphology after breakage, while the adjacent polymer layers were stretched and then curled. Our method produced metallic silver belonging to different layers from top to bottom in one step which is easy to be put into mass production. The rectilinear propagation of UV light ensures the aligning of the building blocks in different layers instead of making alignment marks. Selecting proper irradiation source according to the principle of light diffraction is also crucial for getting matched scale 3D networks.

#### Tracing the silver photo generation process

To understand how the UV curing time affects the silver reduction process, we analyze the reflectance spectra and the film RI value as a function of the UV exposure time. Starting from the  $\text{Ag}^+$  doped 1D ordered layers, the reflectance intensity increased dramatically after 70 min UV exposure from 55% to 85%, as shown in Figure 5a, and the position of Bragg peak was located at 670 nm at last. When compared to the initial state, the position of the stop band blue-shifted which resulted from the broadening of half-peak width.<sup>54</sup> The band width can be calculated by the following equation:

$$W = \frac{4}{\pi} \lambda_{\text{Bragg}} \left| \frac{n_h - n_l}{n_h + n_l} \right|$$

where  $W$  is the band width,  $\lambda_{\text{Bragg}}$  is the peak position,  $n_h$  and  $n_l$  are the refractive index of high-index and low-index layer respectively. As mentioned above, silver NPs increased the refractive index ( $n_h$ ) of PVA layer, thus increased the value of  $(n_h - n_l) / (n_h + n_l)$  resulting in the broadening of the band width. Figure 5b shows the time-dependent change of the reflectance intensity marked by  $\Delta R/R$ , where the value of  $\Delta R$  was defined as the real time reflectance minus the initial reflectance ( $R$ ). The refractive index of the silver composite single film under UV irradiation for various time was shown in the inset of Figure 5b. At the beginning, the reflectance intensity increased linearly, after 45 min UV exposure, it reached a plateau which is in perfect agreement with the rising trend of the single film's RI. The silver composite single film absorption was measured (Figure S5), the intensity of absorption increased with the exposing time. At the beginning, it increased very fast until it reached 20 minutes, which is in good accordance with the change of RI value. The increase of the film absorption verified the rising amount of silver NPs and more NPs brought higher refractive index of the composite film, which resulted in an obvious photonic band. This explains very well that the changing trend of reflection intensity, RI value and absorption intensity matches one another. In order to study whether there is difference between the percentage of silver as reduced metal in top and bottom PVA layers, a group of multilayer samples on quartz glass substrate were prepared. The results are shown in Figure S6 from which we can see that after a certain period UV exposure, most of the silver ions in the

multilayer structure including those embedded in bottom PVA layers are reduced to zero-valent silver metal.

Next, the reflectance spectra and film RI value are measured as a function of silver nitrate doping amount. Figure 6a to 6e shows the reflectance spectra of samples with different amount of  $\text{AgNO}_3$  ranging from 0.01 to 0.05 in the PVA/ $\text{AgNO}_3$  precursor solution ( $\text{g ml}^{-1}$ ) and Figure 6f summarize the changing trend. The larger Ag amount brought higher reflection value before it reached 0.03  $\text{g ml}^{-1}$ . This should be attributed to that more silver ions in the precursor solution would result in larger silver particle fraction in the composite film which lead to higher RI value after photo reduction. On the contrary, further increasing the quantity

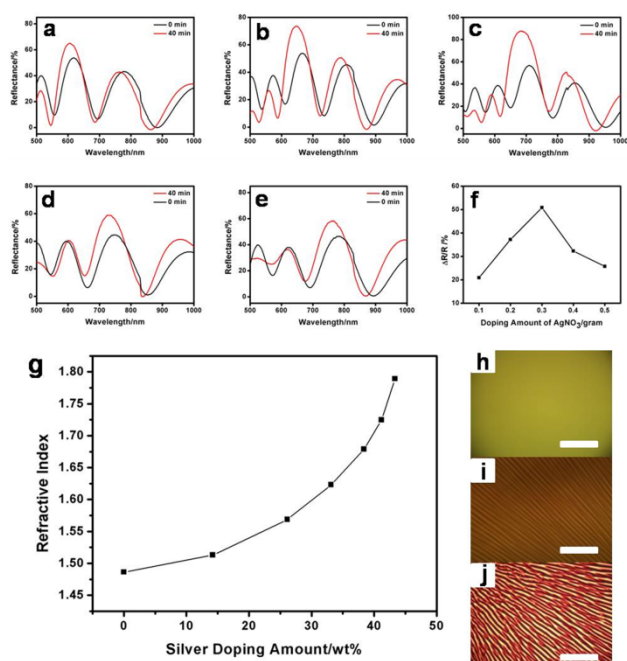


Fig. 6 a) to e) are the reflectance spectra of multilayer structure containing different amount of  $\text{AgNO}_3$  ranging from 0.01 g to 0.05 g dissolved in 1 ml PVA aqueous solution. Black lines represent the original state before UV irradiation while red lines are the reflectance spectra after 40 min UV exposure. f) Summary of the change of the reflectance intensity defined by  $\Delta R/R$  as a function of the  $\text{AgNO}_3$  doping amount ( $\text{g}/10 \text{ ml}$ ). g) The RI values of the silver NPs composite film after UV curing as a function of silver doping amount (atomic weight percentage measured by EDS). h), i), j) are the microphotographs of the composite film containing 0.01, 0.03, 0.05 g silver nitrate in 1 milliliter precursor solution respectively (scale bar are all  $50 \mu\text{m}$ ).

of  $\text{AgNO}_3$  generated the decline of the reflection. This phenomenon can be explained by the phase separation brought by the addition of inorganic silver NPs. Microphotographs of corresponding samples with Ag content in weight percent of 14.2% (h), 33.1% (i), 41.2% (j) in the composite films measured by EDS showed the phase behaviours. A uniform and smooth film was generated from reactive silver-containing precursors followed by *in-situ* photo reduction at lower Ag fraction while higher Ag fraction (above 33.1 wt%) generated stripes which caused by the phase separation in the organic-inorganic composite films. This may increase the light scattering inside the multilayer system and subsequently enhance the energy loss which leading to the decrease of the total reflection. Thus, in following study, we only prepared the composite multilayer structure with silver content no

higher than 33.1 wt% for various tests in order to limit the energy loss in a reasonable level. The refractive indexes of the composite films were measured at 632.8 nm by an ellipsometer (Figure 6g). Starting from 1.4836, the RI value of Ag-contained film reached 1.7892 at 43.35 wt%. We can also see that the RI value has no linear dependence on the Ag weight content which is in good agreement with a previous work on PbS/polymer film.<sup>55</sup> Based on the afore-mentioned discussion, it is clearly that as a high-RI value content, Ag NPs have a great contribution to the increase of the composite films' refractive indexes which produced large contrast between the PVA/Ag layer and the PMMA layer. Higher Ag weight fraction brought higher RI values while larger content inorganic Ag NPs embedded in the polymer film also produced phase separation. Taking both RI and phase performance into consideration, 0.03 g  $\text{AgNO}_3$  in 1 milliliter precursor solution meets both sides and it brought about the strongest reflection among various silver doping amount when other parameters (layer thickness, number of layers and incident angel) are the same.

### Manipulation of the matrix structure

Building a one dimensional layered matrix ahead of 3D construction not only brings the convenience for generating building blocks at one time, but also provides a freely tuning matrix for structural diversity. As we mentioned above, the building of multilayer qualify the material as a real 3D structure, thus total number of layers is one of the key parameters which affects the structural properties. Our 1D matrix can act as a model with convertible number of layers. Increasing the number of layers will add repeating building blocks and thus enhance the mutual interaction inside our 3D structure which is a good model to study. In our 1D layered system, because of the contribution of the Ag NPs to reinforce the RI contrast between the PMMA and PVA layers, increasing layer number will add saturation to

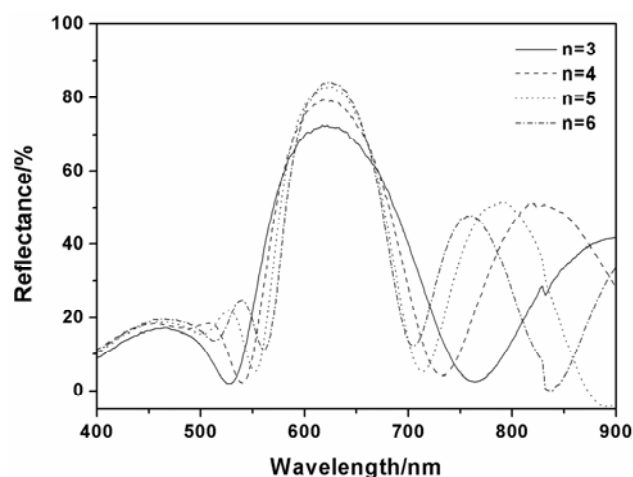


Fig. 7 Adjusting the reflectance intensity of the 1D multilayer structure based on the IDPC theory by varying the number of bilayers (n).

replicate colors more vividly for it enhances the reflection intensity.<sup>56</sup> Figure 7 illustrated the reflectance spectra of the 1D laminar structure with various number of bilayers. For the sample with only 3 bilayers, the reflectance intensity reached 73%, when the number of bilayer increased to 6, an intense peak (above 90%) was observed at 635 nm which had a negligible red shift of the

Bragg peak position and the band width became narrower. The structural measurement by SEM was shown in Figure S7, the sharp interfaces between different layers make it easy for us to distinguish the sample with layer number from 3 to 6, photographs also show that the color saturation of the 6-bilayer sample is the highest among the four samples which brought by the narrower bandwidth and stronger reflection. We also successfully build layered structure with 11 and 14 bilayers, their cross section is shown in Figure S8. There is no dissolution and penetration which indicates that our 1D matrix has good flexibility in changing the total number of consisting layers.

Besides the total number of layers, layer thickness is also crucial to manipulate the layer structure. Usually it can be realized by either vary the polymer solution concentration (*i.e.* the solution viscosity) or the rotation speed/spin time. Here, we first fixed the precursor solution concentration and spin time, lower the rotation speed for each layer by 3000 rpm, 2500 rpm and 2000 rpm to fabricate three samples. The change of the film thickness is reflected by the SEM images and the shift of the peak position.

Cross sectional SEM images are shown in Figure 8a-c. The thicker part is consisted of PVA while the thinner part is PMMA layer. The thickness of PVA layer in Figure 8a-c are 92 nm, 97 nm, 106 nm and the thickness of PMMA layer are 30 nm, 38 nm and 44 nm respectively. The increase of the period thickness resulted in the red shift of the Bragg peak position. As shown in Figure 8d, the peak position was centered at 556 nm, 605 nm and 652 nm respectively which shifted towards the longer wavelength. Photographs in Figure 8d presented vivid color which correspond to the three samples we mentioned above. However, in some cases of stacked 3D structure containing repeating building blocks which have strongly interaction between interval layers, precisely controlling the distance between these layers is highly demand,

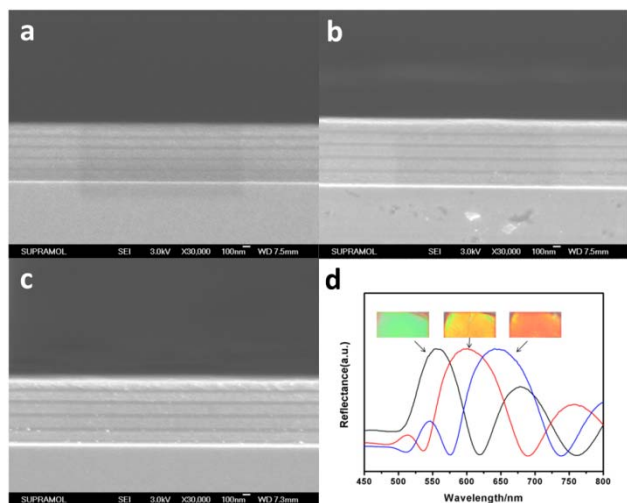


**Fig. 8** Cross sectional SEM images of the 1DPCs consisting of different layer thickness: a) PVA layer is 92 nm and PMMA layer is 30 nm; b) PVA layer is 97 nm and PMMA layer is 38 nm; c) PVA layer is 106 nm and PMMA layer is 44 nm. d) is the corresponding reflectance spectra of the sample a), b) and c) from left to right; insets in Figure 8d are photographs of the three samples (2×1 cm).

*i.e.* the thickness of PMMA layers.<sup>58</sup> To realize this purpose, we spin coat fixed concentration PVA solution together with various

concentration of PMMA solution, the results are shown in Figure S9. SEM images shows the cross section fracture which exhibit clear layer alternative distribution, the PVA layer in all three samples possess the same layer thickness of 102 nm while the thickness of PMMA layer increase from 40, 46 to 53 nm. Using this method, we can freely adjust the thickness of spacer layers to provide a flexible matrix for studying the interaction between building blocks. However, in practical application, we do not need to take SEM measurement to trace the variation of period thickness, it can be verified by the peak red shift in reflectance spectra (Figure S9-d). The adjustments of PVA layer thickness through tuning PVA solution concentration was shown in Figure S10 with fixed PMMA layer thickness of 38 nm and PVA layer thickness varying from 90, 118 to 140 nm. By using the methods we mentioned above, our 1D layered structure proves to be perfect matrix for 3D construction.

## Experimental

### Materials

Poly(vinyl alcohol) (PVA) (Mw 13000-23000) and Poly(methyl methacrylate) (PMMA) with a Mw of 120000 were purchased from Aldrich. Silver nitrate was obtained from Aladdin. All the reagents were used as received without further purification. Silicon wafers (100) were cut into 2×2 cm small pieces followed by cleaning in boiling piranha solution (a mixture of 98% H<sub>2</sub>SO<sub>4</sub> /30% H<sub>2</sub>O<sub>2</sub> with volumetric ratio 7:3, caution: this solution is extremely corrosive!) and then rinsing in DI water for 3 times before use.

### Fabrication of Ag<sup>+</sup> precursor doped 1D heterogeneous layer structure.

The multilayers were fabricated on the as prepared silicon wafers. In detail, PMMA and PVA were first dissolved in toluene and DI water respectively *via* ultrasonic treatment, then adding desired amount of AgNO<sub>3</sub> into the aqueous solution of PVA to form Ag<sup>+</sup> doped precursor solution. The 1D layers were fabricated by spin coating the PVA and PMMA sol alternately at 3000 rpm for 60 s, each layer was baked at 80 °C for 10 min. The first layer was PMMA and the last layer was PVA in all our samples. All the operations were conducted in the dark place to avoid light reduction of the silver ions. The thickness of each layer can be adjusted by changing the concentration of the precursor solution or the rotation speed. The total number of layers was calculated as 2n.

The selection of the solvents to each polymer layer played a very important role in the preparation of pure polymer layered stacks. We chose deionized water for dissolving PVA and silver nitrate together and toluene for dissolving PMMA. Toluene was the excellent solvent for PMMA and poor solvent for PVA which can help form a perfect PMMA thin film without destroying the PVA film. Similarly, deionized water was the excellent solvent for PVA and poor solvent for PMMA which can help form a perfect PVA thin layer without destroying the PMMA layer. The choice of solvents also involved penetrability. In our design, toluene cannot penetrate the PVA layer and deionized water cannot penetrate the PMMA layer which ensured the acquisition of the multilayer 1D matrix.

### In-situ photo reduction of Ag<sup>+</sup> to form Ag NPs inside layer structure

Silver NPs were formed by exposing the as prepared laminar structure sample to UV irradiation (500 W,  $\lambda = 365$  nm) for preset time in room temperature. The UV curing system was equipped with an ACM mirror and cooling system for temperature reduction.

### Photo induced 3D frameworks inside 1D layer stacks

The 3D structure contained silver skeleton was produced by UV reduction of the sample with a pre-designed photomask. Based on different pattern of the photomask, the silver skeleton formed inside every PVA layer will exhibit corresponding stripes, dots, triangle and English letters. During the exposing process, the mask is strictly fixed on top of the 1D layer stacks to ensure the alignment of the silver NPs from the sample surface to the bottom, thus formed a perfect skeleton inside the 1DPC.

### Finite-Difference Time-Domain (FDTD) calculations

The calculated reflectance spectra were obtained using the commercialized software package, FDTD Solutions (Lumerical Solutions, Inc., Canada). A two-dimensional simulation region was employed on XY plane. A Periodic boundary condition was set in  $\pm Y$  direction and two perfectly matched layers in  $\pm X$  direction. The incident plane waves were perpendicular to sample surfaces. The layer thicknesses and refractive indexes of the simulation models were set according to those of corresponding fabricated samples.

### Characterization

A Shimadzu 3600 UV-VIS-NIR spectrophotometer was used to measure the absorbance and reflectance spectra. The cross sectional micrographs were taken by JEOL FESEM 6700F scanning electron microscope (SEM), all the samples were sputtered with a thin layer of Pt before test. The size of the photoreduced silver nanoparticles was determined by a Hitachi H-800 transmission electron microscope (TEM). An Electronic Data Systems (EDS) analyzer attached to the JEOL FESEM 6700F scanning electron microscope operating in the SEI mode was used to analyze the Ag formed in the composite films. An X-ray photoelectron (XPS) test using Mg K  $\alpha$  excitation (1253.6 eV) to the silver-contained composite films was collected in a VG ESCALAB MKII spectrometer. Binding energy calibration was based on C 1s at 284.6 eV. The thickness of PVA and PMMA single layer was measured by Dektak 150 surface profiler (Veeco). The refractive indices of the polymer thin films at the wavelength of 632.8 nm were measured on an AUER-III auto-laser ellipsometer equipped with a He-Ne laser ( $\lambda = 632.8$  nm). The micro photographs were taken by Olympus BX 51. Digital camera photographs were shot by Canon Powershot G1X.

### Conclusion

The 3D ordered structure has been constructed by conducting a photo-reduction process in a Ag ions doped heterogeneous 1D structure. Employing this reaction between UV light and Ag<sup>+</sup> opens up a new way to fabricate 3D networks inside the multilayer. By selectively photo reducing the part without protection, our method realize the formation of Ag NPs belonging

to different layers in one step. The alignment of the silver building blocks belonging to different layers is simply guaranteed by the rectilinear propagation of UV light instead of complex and repeating aligning process. The embedded silver NPs also dramatically increase the refractive index value of PVA layers, thus result in an obvious PBG with less layers, which provides us a method to trace the silver formation process. The number of layers and the distance between adjacent silver lattice layers can be precisely tuned as needed. For chasing more delicate structure, shorter wavelength light should be applied as the radiation source to produce the building blocks with much smaller size by avoiding the light diffraction. We believe that further study will help reveal the potential use of our structure in the fields such as bioassays, SERS matrix and especially photonic *meta*-material with working frequency at optical range can be envisioned based on our chemical approaches.

### Acknowledgement

This work was financially supported by the National Science Foundation of China (NSFC) under Grant No. 91123031, 21221063, 51373065 and the National Basic Research Program of China (973 Program) under Grant No. 2012CB933800.

### Notes and references

<sup>a</sup> State Key Laboratory of Supramolecular Structure and Materials, College of Chemistry, Jilin University, Changchun, 130012, P. R. China. E-mail: byangchem@jlu.edu.cn

<sup>b</sup> Laboratory of Organic Chemistry, Wageningen University and Research Center, Dreijenplein 8, 6703 HB, Wageningen, The Netherlands. E-mail: wzh12020915@gmail.com

† Electronic Supplementary Information (ESI) available: Detailed characterization of the patterned sample, SEM measurement of the 3D structure, absorbance spectrum of single composite film and structural variation as function of layer numbers and layer thickness respectively were given. See DOI: 10.1039/b000000x/

1. D. G. Stavenga, S. Foletti, G. Palasantzas and K. Arikawa, *Proc. R. Soc. London, Ser. B.*, 2006, **273**, 661.
2. M. Srinivasarao, *Chem. Rev.*, 1999, **99**, 1935.
3. P. Vukusic and J. R. Sambles, *Nature*, 2003, **424**, 852.
4. A. R. Parker and H. E. Townley, *Nat. Nanotechnol.*, 2007, **2**, 347.
5. Q. F. Cheng, M. Z. Li, L. Jiang and Z. Y. Tang, *Adv. Mater.*, 2012, **24**, 1838.
6. J. G. Fleming and S. Y. Lin, *Opt. Lett.*, 1999, **24**, 49.
7. O. Jeon and E. Alsborg, *Adv. Funct. Mater.*, 2013, **23**, 4765.
8. J. Valentine, S. Zhang, T. Zentgraf, E. Ulin-Avila, D. A. Genov, G. Bartal and X. Zhang, *Nature*, 2008, **455**, 376.
9. N. Liu, H. C. Guo, L. W. Fu, S. Kaiser, H. Schweizer and H. Giessen, *Nat. Mater.*, 2008, **7**, 31.
10. J. X. Wang, Y. Z. Zhang, S. T. Wang, Y. L. Song and L. Jiang, *Acc. Chem. Res.*, 2011, **44**, 405.
11. A. Biswas, I. S. Bayer, A. S. Biris, T. Wang, E. Dervishi and F. Faupel, *Adv. Colloid Interface Sci.*, 2012, **170**, 2.
12. J. E. E. Baglin, *Appl. Surf. Sci.*, 2012, **258**, 4103.
13. Y. L. Zhang, Q. D. Chen, H. Xia and H. B. Sun, *Nano Today*, 2010, **5**, 435.

14. S. M. George, *Chem. Rev.*, 2010, **110**, 111.
15. R. W. J. Scott, S. M. Yang, N. Coombs, G. A. Ozin and D. E. Williams, *Adv. Funct. Mater.*, 2003, **13**, 225.
16. B. Su, S. T. Wang, Y. C. Wu, X. Chen, Y. L. Song and L. Jiang, *Adv. Mater.*, 2012, **24**, 2780.
17. G. R. Xiong, G. Z. Han, C. Sun, H. Xu, H. M. Wei and Z. Z. Gu, *Adv. Funct. Mater.*, 2009, **19**, 1082.
18. J. Liu, Y. Mao and J. Ge, *Nanoscale*, 2012, **4**, 1598.
19. Y. Aizawa, R. Wylie and M. Shoichet, *Adv. Mater.*, 2010, **22**, 4831.
20. M. E. Kolewe, H. Park, C. Gray, X. F. Ye, R. Langer and L. E. Freed, *Adv. Mater.*, 2013, **25**, 4459.
21. W. H. Peng, S. M. Zhu, W. L. Wang, W. Zhang, J. J. Gu, X. B. Hu, D. Zhang and Z. X. Chen, *Adv. Funct. Mater.*, 2012, **22**, 2072.
22. D. R. Smith, W. J. Padilla, D. C. Vier, S. C. Nemat-Nasser and S. Schultz, *Phys. Rev. Lett.*, 2000, **84**, 4184.
23. C. M. Soukoulis, S. Linden and M. Wegener, *Science*, 2007, **315**, 47.
24. C. M. Soukoulis and M. Wegener, *Science*, 2010, **330**, 1633.
25. C. R. Simovski, P. A. Belov, A. V. Atrashchenko and Y. S. Kivshar, *Adv. Mater.*, 2012, **24**, 4229.
26. H. O. Moser and C. Rockstuhl, *Laser Photonics Rev.*, 2012, **6**, 219.
27. F. Monticone and A. Alù, *Chin. Phys. B.*, 2014, **23**, 047809.
28. Z. Li, M. Mutlu and E. Ozbay, *J. Opt.*, 2013, **15**, 023001.
29. M. Kadic, T. Bückmann, R. Schittny and M. Wegener, *Rep. Prog. Phys.*, 2013, **76**, 126501.
30. J.-H. Lee, J. P. Singer and E. L. Thomas, *Adv. Mater.*, 2012, **24**, 4782.
31. C. M. Soukoulis and M. Wegener, *Nat. Photonics.*, 2011, **5**, 523.
32. D. R. Clary and G. Mills, *J. Phys. Chem. C*, 2011, **115**, 14656.
33. J. G. Zhang, S. Q. Xu and E. Kumacheva, *Adv. Mater.*, 2005, **17**, 2336.
34. K. K. Chia, R. E. Cohen and M. F. Rubner, *Chem. Mater.*, 2008, **20**, 6756.
35. G. Machado, M. M. Beppu, A. F. Feil, C. A. Figueroa, R. R. B. Correia and S. R. Teixeira, *J. Phys. Chem. C*, 2009, **113**, 19005.
36. A. S. Korchev, T. Konvalova, V. Cammarata, L. Kispert, L. Slaten and G. Mills, *Langmuir*, 2006, **22**, 375.
37. G. A. Gaddy, A. S. Korchev, J. L. McLain, B. L. Slaten, E. S. Steigerwalt and G. Mills, *J. Phys. Chem. B*, 2004, **108**, 14850.
38. B. V. Lotsch, C. B. Knobbe and G. A. Ozin, *Small*, 2009, **5**, 1498.
39. T. A. Baker, O. L. A. Monti and D. J. Nesbitt, *J. Phys. Chem. C*, 2011, **115**, 9861.
40. A. S. Korchev, M. J. Bozack, B. L. Slaten and G. Mills, *J. Am. Chem. Soc.*, 2004, **126**, 10.
41. N. Marquestaut, Y. Petit, A. Royon, P. Mounaix, T. Cardinal and L. Canioni, *Adv. Funct. Mater.*, 2014, **24**, 5824.
42. K. Shimizu and A. Satsuma, *PCCP*, 2006, **8**, 2677.
43. T. V. Slenters, I. Hauser-Gerspach, A. U. Daniels and K. M. Fromm, *J. Mater. Chem.*, 2008, **18**, 5359.
44. N. Leopold and B. Lendl, *J. Phys. Chem. B*, 2003, **107**, 5723.
45. A. Klinkova, R. M. Choueiri and E. Kumacheva, *Chem. Soc. Rev.*, 2014, **43**, 3976.
46. N. Liu, H. Guo, L. Fu, S. Kaiser, H. Schweizer and H. Giessen, *Nat. Mater.*, 2007, **7**, 31.
47. Z. Wang, J. Zhang, J. Xie, Z. Wang, Y. Yin, J. Li, Y. Li, S. Liang, L. Zhang, L. Cui, H. Zhang and B. Yang, *J. Mater. Chem.*, 2012, **22**, 7887.
48. D. Owens, C. Fuentes-Hernandez and B. Kippelen, *Thin Solid Films*, 2009, **517**, 2736.
49. H. Kong and J. Jang, *Chem. Commun.*, 2006, 3010.
50. J. Zeng, C. Zhu, J. Tao, M. S. Jin, H. Zhang, Z. Y. Li, Y. M. Zhu and Y. N. Xia, *Angew. Chem. Int. Ed.*, 2012, **51**, 2354.
51. K. Yu, X. Y. Liu, Q. Zeng, M. L. Yang, J. Y. Ouyang, X. Q. Wang and Y. Tao, *Angew. Chem. Int. Ed.*, 2013, **52**, 11034.
52. Y. Zhou, S. H. Yu, C. Y. Wang, X. G. Li, Y. R. Zhu and Z. Y. Chen, *Adv. Mater.*, 1999, **11**, 850.
53. C. Damm, H. Münstedt, *Appl. Phys. A*, 2008, **91**, 479.
54. E. Redel, J. Mlynarski, J. Moir, A. Jelle, C. Huai, S. Petrov, M. G. Helander, F. C. Peiris, G. von Freymann and G. A. Ozin, *Adv. Mater.*, 2012, **24**, OP265.
55. C. L. Lu, C. Guan, Y. F. Liu, Y. R. Cheng and B. Yang, *Chem. Mater.*, 2005, **17**, 2448.
56. V. A. Tolmachev, A. V. Baldycheva, E. Y. Krutkova, T. S. Perova and K. Berwick, *Modeling Aspects in Optical Metrology II*, 2009, **7390**, 739017.
57. A. E. Miroshnichenko, B. Luk'yanchuk, S. A. Maier and Y. S. Kivshar, *ACS Nano*, 2012, **6**, 837.
58. C. Garcia-Meca, J. Hurtado, J. Marti, A. Martinez, W. Dickson and A. V. Zayats, *Phys. Rev. Lett.*, 2011, **106**, 067402.

## From 1D to 3D: A New Route to Fabricate Tridimensional Structure *via* Photo Generation of Silver Networks

Huaizhong Shen,<sup>a</sup> Yuxin Wu,<sup>a</sup> Liping Fang,<sup>a</sup> Shunsheng Ye,<sup>a</sup> Zhaoyi Wang,<sup>a</sup> Wendong Liu,<sup>a</sup> Zhongkai Cheng,<sup>a</sup> Junhu Zhang,<sup>a</sup> Zhanhua Wang\*<sup>b</sup> and Bai Yang\*<sup>a</sup>

<sup>a</sup> State Key Laboratory of Supramolecular Structure and Materials, College of Chemistry, Jilin University, Changchun, 130012, P. R. China. E-mail:

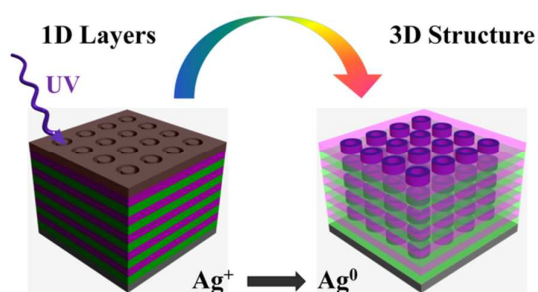
byangchem@jlu.edu.cn

<sup>b</sup> Laboratory of Organic Chemistry, Wageningen University and Research Center, Dreijenplein 8, 6703 HB, Wageningen, The Netherlands. E-mail:

wzh12020915@gmail.com

### Table of Contents Graphic

Three dimensional ordered structure is of great importance for its wide applications such as light manipulation and tissue engineering. A time-saving and low-cost method is established to construct 3D structure through the combination of bottom-up and top-down technology which enable us to create the building blocks freely and to precisely adjust the matrix feature.



A novel method is established to construct stacked 3D structure by *in-situ* reducing silver ions inside a 1D layer matrix.